

# Ordered Mesostructured CdS Nanowire Arrays with Rectifying Properties

Na Yuan · Gang Cheng · Yanqing An ·  
Zuliang Du · Sixin Wu

Received: 14 November 2008 / Accepted: 30 December 2008 / Published online: 6 February 2009  
© to the authors 2009

**Abstract** Highly ordered mesoporous CdS nanowire arrays were synthesized by using mesoporous silica as hard template and cadmium xanthate ( $\text{CdR}_2$ ) as a single precursor. Upon etching silica, mesoporous CdS nanowire arrays were produced with a yield as high as 93 wt%. The nanowire arrays were characterized by XRD,  $\text{N}_2$  adsorption, TEM, and SEM. The results show that the CdS products replicated from the mesoporous silica SBA-15 hard template possess highly ordered hexagonal mesostructure and fiber-like morphology, analogous to the mother template. The current–voltage characteristics of CdS nanoarrays are strongly nonlinear and asymmetrical, showing rectifying diode-like behavior.

**Keywords** Nanomaterials · CdS · Nanowire arrays · SBA-15 · Rectification

## Introduction

Efforts in nanomaterials have rapidly expanded into the assembly of well-ordered two- and/or three-dimensional (2D and/or 3D) superstructures. The 3D superstructures provide possibilities to probe brand-new properties and applications due to the spatial orientation and arrangement of the nanocrystals [1–3]. Different methods have been used to fabricate preferentially oriented nanowire arrays, such as, electrodeposition [4–6], vapor–liquid–solid (VLS) [7, 8], thermal evaporation [9–11], lithography [12, 13], AAO [14, 15], or mesoporous silica SBA-15 [16]-assisted

methods. In these methods, SBA-15 template shows a promising technique in controlling the preferential orientation without changing the nanowire morphology, and it has been explored for synthesis of Ag, Au, Pt, Ph, and Si nanowires [17, 18] as well as binary semiconductor nanowires [19–22]. As previously reported, after removal of the silica template, the ordered mesostructure is seldom maintained, because the inorganic precursors are inclined to be absorbed on the external surface of templates and the channels are not completely filled up, which causes the framework formed inside the pores to be lacking in sufficient internal cross-linkage.

Recently, a single-source precursor, cadmium thioglycolate, was used to synthesize crystalline mesoporous CdS nanoarrays through SBA-15 silica template technique [23]. The results demonstrated that such mesoporous semiconductor nanoarrays with high crystallinity were exactly an inverse replica of SBA-15.

These nanoarrays provide many opportunities for new applications as advanced materials; however, the systematic studies of the transport, optical, and electrical properties of these nanoarrays were not reported till now.

It is known that the rectification is of great importance in modern electronic applications [24]. Recently, some research has focused on rectification properties in the nanoscale [25–27]. The electrical properties of CdS with different morphologies, such as nanoparticles [28], nanorods [29], and nanowires [30], were reported recently. The  $I$ – $V$  characterization of these CdS systems demonstrated good ohmic contacts [29, 31] or highly insulating [30, 32], but the rectification was not observed in these pure CdS systems. The rectification can be obtained only when CdS form heterostructures with others, such as, nanoparticles [28], polymer [30, 32] or Si [33]. Here, the CdS nanoarrays were synthesized through single-source precursor, metal

N. Yuan · G. Cheng · Y. An · Z. Du · S. Wu (✉)  
Key Laboratory of Special Functional Materials, Henan  
University, Kaifeng 475001, People's Republic of China  
e-mail: wusixin@henu.edu.cn

alkyl xanthate [34]. The remarkable performance on rectification within a bundle of CdS nanoarrays was characterized by semiconductor characteristic measurement system (Keithley 4200 SCS), and the mechanism of the rectification of the CdS nanoarrays was discussed.

## Experimental

Mesoporous silica SBA-15 was prepared by a triblock copolymer under hydrothermal treatment at 130 °C for 48 h following the general procedure reported by Zhao et al. [16]. For synthesis of CdS nanoarrays, typically, 0.05 g SBA-15 was added to a solution obtained by dissolving 0.34 g of cadmium alkyl xanthate in a certain amount of tetrahydrofuran, and then the mixture was kept stirring at room temperature until the solvent was completely vaporized. The residual powders were dried and then heated to 160 °C at a rate of 1 °C/min and maintained at this temperature for 10 h under argon. The powders turned yellow during the thermal treatment process. The obtained cadmium sulfide–silica composites were soaked in 2 M NaOH for several hours to remove the silica template. The template-free CdS products were recovered by centrifugation, washed with water, and dried at room temperature.

The morphology of the samples was characterized by transmission electron microscope (TEM, JEM-100CX) at 100 kV. Structural characterization was performed by X-ray diffraction (XRD, X'Pert Pro MPD, with Cu K $\alpha$  radiation,  $\lambda = 1.54060 \text{ \AA}$ ) at 40 kV and 40 mA. Scanning electron microscope (SEM) measurement was carried out using a JSM-5600 LV equipped with EDX (Oxford ISIS) at 20 kV. The  $I$ - $V$  curves of assembled CdS nanowire arrays were measured by semiconductor characteristic system (Keithley 4200-SCS) at 350 nm illumination. Nitrogen adsorption–desorption isotherms were measured on a Micromeritics Tristars 3000 analyzer at  $-196 \text{ }^\circ\text{C}$ . Before the measurements, the samples were degassed at 160 °C for 6 h in vacuum.

## Results and Discussion

The SBA-15 was synthesized at a high hydrothermal temperature of 130 °C to increase the mesotunnels, which are beneficial for the production of high-quality replica materials. Figure 1a exhibits the small-angle X-Ray diffraction of the template-free CdS nanoarrays. The small-angle regions show three well-resolved diffraction peaks. It indicates a highly ordered 2D hexagonal mesostructure; at the same time, it implies that CdS nanoarrays replicate well the ordered mesoporous of the SBA-15 template and

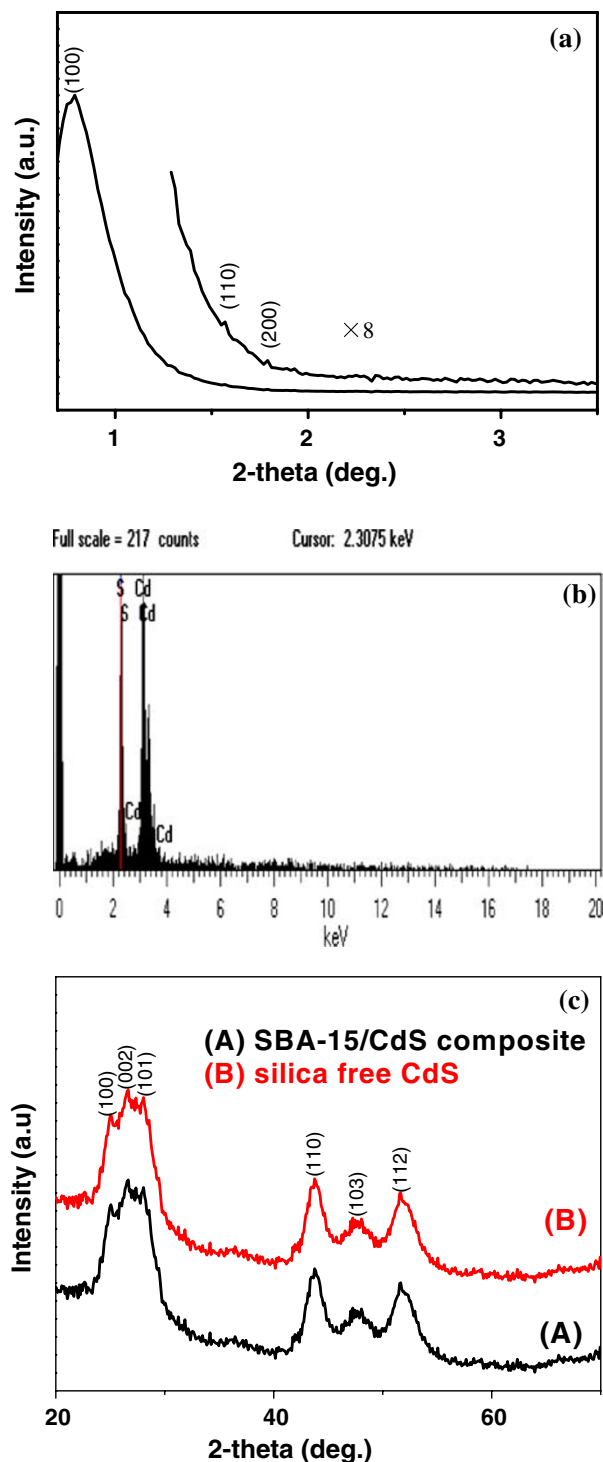


**Fig. 1** a Small-angle diffraction pattern of template-free CdS nanoarrays. b EDS pattern of the template-free CdS nanoarrays. c WAXD diffraction curves of CdS nanoarrays present in SBA-15 pore channels and silica-free CdS nanoarrays

confirms the ordered arrangement of CdS nanowires [23]. The EDX spectrum of the nanowire arrays confirms that these nanowire arrays consist of stoichiometric CdS with a Cd/S ratio of 1.05:1 and displays strong signals from Cd to

S elements without the detection of silicon element. It also indicates the complete removal of the silica scaffold (Fig. 1b).

The wide-angle XRD patterns of the CdS nanoarrays (Fig. 1c) before and after removal of SBA-15 show the (100), (002), (101), (110), (103), and (112) planes at  $2\theta$  values 24.8°, 26.5°, 28.2°, 43.7°, 47.8°, and 51.8°, respectively, which match those of the hexagonal wurtzite structure of CdS crystallite. The same XRD patterns of CdS nanoarrays before and after removal of SBA-15 template demonstrated that the structure of the CdS nanoarrays is completely maintained during the etching. On the basis of the width of the diffraction peaks, the size of the CdS nanocrystals is on the nanometer scale and the average particle size is calculated to be 7.1 nm, which is consistent with the pore diameter of the host SBA-15.

Figure 2 shows the nitrogen sorption isotherms (Fig. 2a) and pore size distribution (Fig. 2b) of the materials

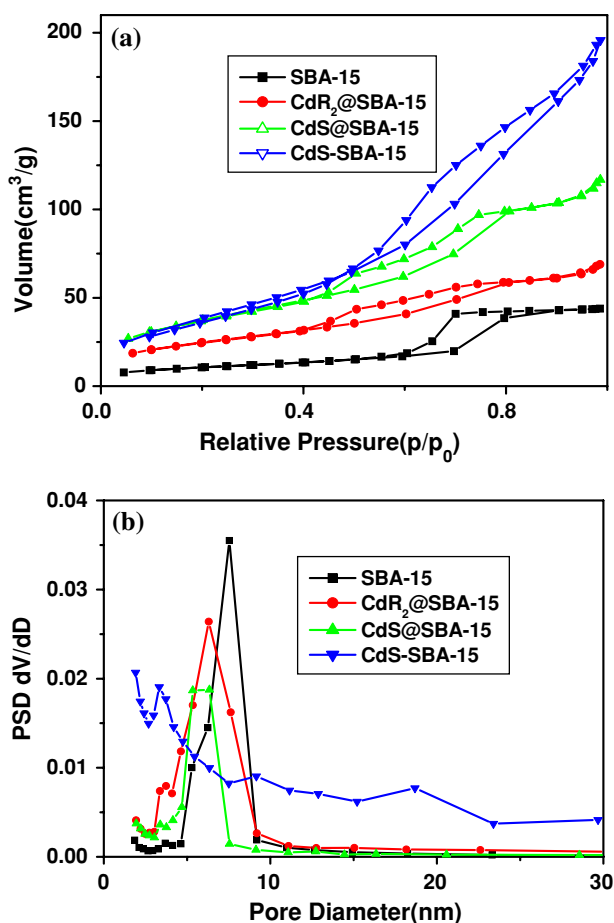
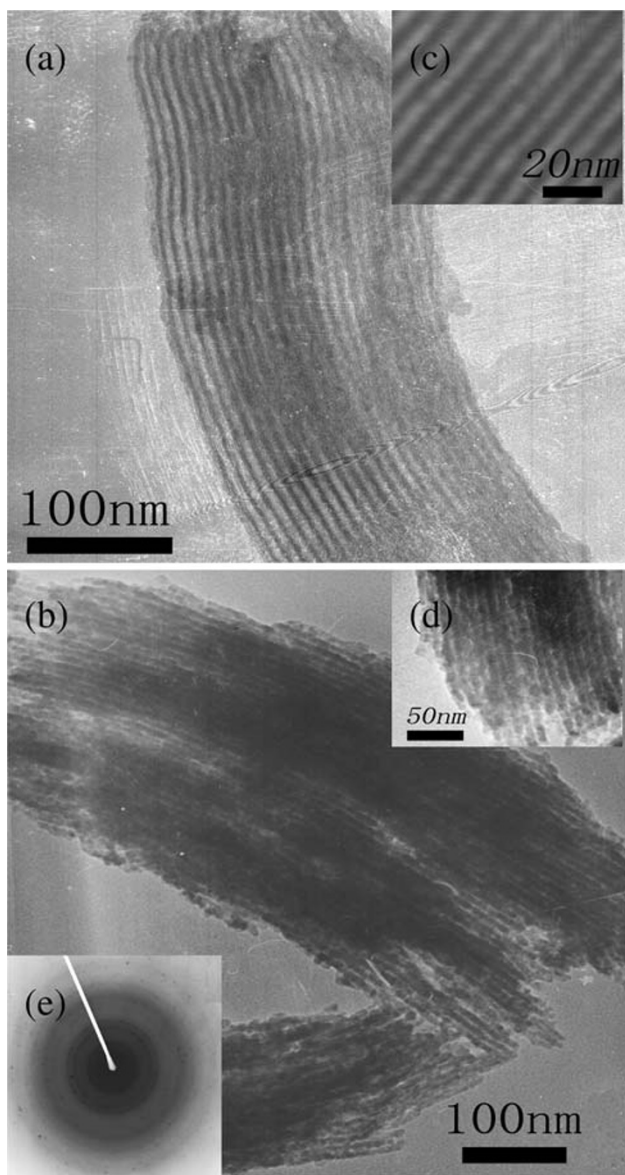


**Fig. 2** **a** Nitrogen sorption isotherms of the samples successively produced in the synthesis: the SBA-15 hard template (■), CdR<sub>2</sub>@SBA-15 composites (●) prepared by the impregnation of CdR<sub>2</sub> into SBA-15, CdS@SBA-15 (▲) obtained from the CdR<sub>2</sub>@SBA-15 calcined at 160 °C, and CdS-SBA-15 replicas (▼) etched by NaOH solution. **b** The corresponding pore-size distribution curves of **a**

successively obtained in the synthesis process, respectively. The isotherms of the SBA-15 template (Fig. 2a) show typical type-IV curves with an H1-type hysteresis loop, attributed to perfect cylindrical mesopore channels. A calcined mesoporous silica sample exhibits a high surface area of 560 m<sup>2</sup>/g, the pore volume of 1.23 cm<sup>3</sup>/g, and a narrow pore size distribution with a mean value of 7.3 nm. The surface area and pore size distribution of the CdR<sub>2</sub>/SBA-15 nanocomposite are 28 m<sup>2</sup>/g and 5.4 nm, respectively, and the adsorption volume is 0.06 cm<sup>3</sup>/g, suppressed by 20 times after the one-step nanocasting process. Upon the calcination at 160 °C for CdS@SBA-15, the surface area and the pore volume decrease to 38 m<sup>2</sup>/g and 0.04 cm<sup>3</sup>/g, respectively, suggesting that the pores have been filled up by CdR<sub>2</sub>. Nitrogen absorption-desorption isotherms for the template-free CdS sample exhibit a surface area of 100 m<sup>2</sup>/g and a pore volume of 0.11 cm<sup>3</sup>/g. A relatively narrow pore size distribution of around 3.3 nm is also exhibited, further demonstrating the high-quality mesoporous CdS replicas.

Figure 3 demonstrates the TEM images of the SBA-15 template, and the CdS nanoarrays after the removal of SBA-15 templates (Fig. 3a and b), respectively. The TEM images reveal that SBA-15 (Fig. 3a) templates have a uniform fiber-like morphology and well-ordered 2D mesoporous structures with uniform pore size. The high-magnification TEM shows the pore size of SBA-15 to be approximately 7.3 nm (Fig. 3c). The representative TEM images (Fig. 3b) demonstrate that the as-prepared CdS nanowire arrays have a uniform fiber-like morphology, and that the length of the CdS nanowire arrays to be more than 2 μm. From the insert of Fig. 3b, it is obviously observed that these CdS nanowire arrays are composed of uniform nanowire, and the diameter of each nanowire is about 7.3 nm, which is in reasonable agreement with the mean pore size of the silica template. These phenomena may reflect that the CdS nanowire arrays are perfect duplication of the hard template and a high yield for the incorporation of CdS. The selected-area electron diffraction (SAED) pattern (Fig. 3e) observed from this area can be indexed as the hexagonal wurtzite CdS structure, indicating that the products consist of wurtzite CdS nanocrystals, which is in agreement with the XRD data.

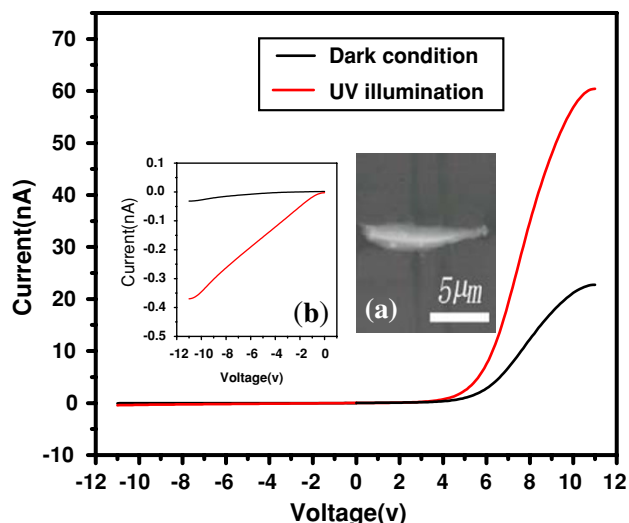
In recent years, AC electric field assembly is widely used to construct nanodevices from nanowires [35, 36] and carbon nanotubes [37–39]. Here, the CdS nanowire arrays were ultrasonically dispersed in ethanol. After applying a droplet of the nanowire arrays suspension onto the electrodes, the Pt electrodes were connected to an 8-V<sub>pp</sub> (peak-to-peak) and 10-kHz AC signal for 30 s. This signal generated an alternating electrostatic force on the nanowire arrays in the solution. Under the electrical polarization force, the nanowire arrays were deposited on the



**Fig. 3** **a** TEM images of the SBA-15 sample along the direction of the hexagonal pore arrangement. **b** TEM images of the template-free CdS sample. Inset **c** and **d** are corresponding High-magnification TEM images. Inset **e** is the corresponding SAED pattern of **b**

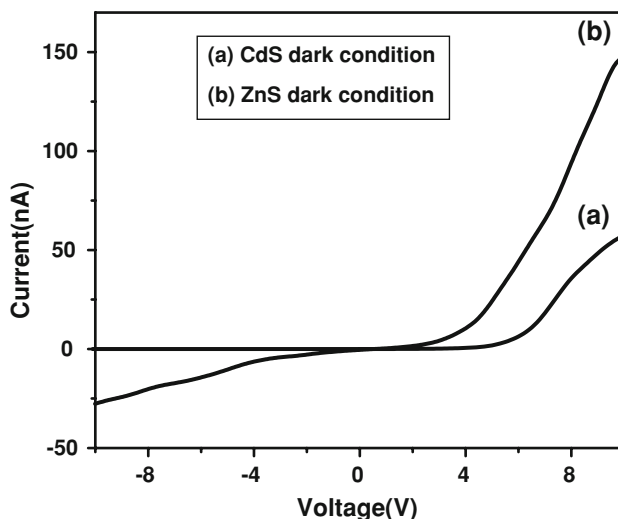
electrodes. The 10-nm-thick Pt electrodes were patterned on an oxidized silicon wafer with 200-nm silicon dioxide using photolithography. The Fig. 4a shows the SEM image of a bundle of CdS nanowire arrays on Pt electrodes. The electrical transport property was carried out through semiconductor characterization system (KEITHLEY 4200-SCS).

Figure 4 shows the *I*–*V* curves of the assembled CdS nanowire arrays under dark and illumination conditions. The *I*–*V* measurement shows a nonlinear characteristic. Little current flows in reverse bias, whereas, the current increases rapidly when the bias voltage is more than 4 V.



**Fig. 4** The *I*–*V* curves of CdS nanowire arrays at dark and uv-illumination condition. Inset **a** is the SEM image of a bundle of CdS nanowire arrays on Pt electrodes. Inset **b** is the detailed *I*–*V* characteristic of the CdS nanowire arrays under reverse bias

The most striking feature (Fig. 4) is that both of the curves display rectifying behaviors at room temperature in air environment. Under dark condition, this rectifying diode-like behavior has a threshold voltage of  $\sim 3.9$  V, and no obvious breakdown current is observed even at  $-11$  V bias. The reverse leakage current is only 0.04 nA at  $-11$  V (Fig. 4b); at the same time, the forward current is 25 nA at 11 V, and their rectification ratio is about 625. Under UV ( $\lambda = 350$  nm)-illumination the turn-on voltage was dropped from 3.9 V to 3.4 V, and the breakdown current is not observed even at  $-11$  V bias. The reverse current is 0.42 nA at  $-11$  V, the forward current is 64 nA at 11 V, and their rectification ratio is about 152.



**Fig. 5** The *I*–*V* curves of CdS **(a)** and ZnS **(b)** nanoarrays at dark condition

The rectifying behavior is an important application of a diode [25–27]. Recently, the rectifying behaviors of electric field-assembled ZnO nanowire have been reported [40]. To our knowledge, such rectifying behaviors were not reported in pure CdS system. In order to confirm the validity of the rectification for different metal sulfides, ZnS nanoarrays were prepared with the same template system. The experimental results are illustrated in Fig. 5b. Under dark condition, we observed the threshold voltage of  $\sim 2.0$  V, the forward current of 150 nA at 10 V, and the reverse current of 27 nA at  $-10$  V. For CdS nanoarrays (Fig. 4b), the reverse current is just 0.04 nA at  $-11$  V, and the reverse current for ZnS nanoarrays is much larger than that of CdS nanoarrays, so the rectification ratio for ZnS nanoarrays is about six. But the obvious rectifying characterization was observed from the ZnS nanowire arrays. It is a very effective method for preparing metal sulfides with rectification through SBA-15 as hard template and using a single-source precursor. How can rectification be formed in these metal sulfide nanoarrays?

According to our previous reports on the current transport behavior of semiconductor nanowires [41, 42], the nonlinear transport behavior in Fig. 4 indicates that the CdS nanoarrays make two Schottky barrier contacts with the two Pt electrodes, and a back-to-back Schottky barriers structure is formed. In brief, the back-to-back Schottky barrier structure is composed of two inversely connected Schottky barriers, and the current in this structure is dominated by the reverse current of the reverse-biased Schottky barrier. The detailed description of the properties of the back-to-back Schottky barriers structure has been discussed in the previous reports of our group [41, 42] and other groups [43, 44]. In this structure, there should be no rectifying behavior if the two Schottky barrier were symmetric. However, in the dielectrophoresis deposition process, the AC voltage introduces an electrostatic force on the nanoarrays, and then the nanoarrays move toward the electrodes until it gets finally deposited on them. The contacts of both ends of the nanoarrays onto the electrodes occur in a consecutive order. We consider that the side of the nanoarrays that touched the electrode first may have a firm contact with the electrode, thus forming a better contact with lower barrier height, whereas the other end that contacted later had a higher barrier, possibly leading to the formation of the Schottky diode for our devices. Thus, the asymmetric contacts were formed between the CdS nanoarrays and Pt electrodes, and resulted in the rectifying behavior. Similar rectifying behaviors have been reported in some systems [7, 45].

There occurs a current difference between the dark and UV illumination, because more number of electrons in the valence band are excited into the conduction band under UV illumination thereby increasing the carrier concentration of

the CdS nanowire arrays. As shown in Fig. 4, both the  $I$ – $V$  curves under dark and illumination conditions show linear behaviors when the bias is larger than 6 V. In this linear region, the current transport property is dominated by the nanowire itself, not by the Schottky barrier. The slope of this linear region is proportional to the carrier concentration of the CdS nanowire arrays. As shown in Fig. 4, the slope of the current curve under illumination condition is three times higher than that of the one under dark condition. This high photocurrent response shows the promising applications of the CdS nanoarray as photodetector.

## Conclusions

In summary, highly ordered mesoporous CdS nanoarrays have been achieved by SBA-15 as a template and cadmium xanthate as a single-source precursor. These materials exist as strongly nonlinear and asymmetrical, showing rectifying diode-like behavior, and provide opportunities for new applications as advanced nanodevices. The synthesis and properties of other systems, such as, MnS, ZnS/CdS composite nanoarrays, are currently in process.

**Acknowledgment** This study was supported by Henan Project for University Prominent Research Talents (HAIPURT) (Grant No. 2007KYCX0012).

## References

1. I. Willner, F. Patolsky, J. Wasserman, *Angew. Chem. Int. Ed.* **40**, 1861 (2001). doi:10.1002/1521-3773(20010518)40:10<1861::AID-ANIE1861>3.0.CO;2-V
2. H. Zheng, J. Wang, S.E. Lofland, Z. Ma, L. Mohaddes-Ardabili, T. Zhao, L. Salamanca-Riba, S.R. Shinde, S.B. Ogale, F. Bai, D. Viehland, Y. Jia, D.G. Schlom, M. Wuttig, A. Roytburd, R. Ramesh, *Science* **303**, 661 (2004). doi:10.1126/science.1094207
3. K.M. Ainslie, G. Sharma, M.A. Dyer, C.A. Grimes, M.V. Pishko, *Nano Lett.* **5**, 1852 (2005). doi:10.1021/nl051117u
4. D. Routkevitch, T. Bigioni, M. Moskovits, J.M. Xu, *J. Phys. Chem.* **100**, 140 (1996). doi:10.1021/jp952910m
5. F.H. Xue, G.T. Fei, B. Wu, P. Cui, L.D. Zhang, *J. Am. Chem. Soc.* **127**, 153 (2005). doi:10.1021/ja0547073
6. Y. Yang, S.C. Kung, D.K. Taggart, C. Xiang, F. Yang, M.A. Brown, A.G. Güell, T.J. Kruse, J.C. Hemminger, R.M. Penner, *Nano Lett.* **8**, 2447 (2008). doi:10.1021/nl801442c
7. G.D. Yuan, W.J. Zhang, J.S. Jie, X. Fan, J.A. Zapien, Y.H. Leung, L.B. Luo, P.F. Wang, C.S. Lee, S.T. Lee, *Nano Lett.* **8**, 2591 (2008). doi:10.1021/nl073022t
8. T. Henry, K. Kim, Z. Ren, C. Yerino, J. Han, H.X. Tang, *Nano Lett.* **7**, 3315 (2007). doi:10.1021/nl071530x
9. J.J. Niu, J.N. Wang, *J. Phys. Chem. B* **111**, 4368 (2007). doi:10.1021/jp070682d
10. B. Xiang, P. Wang, X. Zhang, S.A. Dayeh, D.P.R. Aplin, C. Soci, D. Yu, D. Wang, *Nano Lett.* **7**, 323 (2007). doi:10.1021/nl062410c
11. J.P. Ge, Y.D. Li, *Adv. Funct. Mater.* **14**, 157 (2004). doi:10.1002/adfm.200305051

12. X.M. Yan, S. Kwon, A.M. Contreras, J. Bokor, G.A. Somorjai, *Nano Lett.* **5**, 745 (2005). doi:[10.1021/nl050228q](https://doi.org/10.1021/nl050228q)
13. T. Martensson, P. Carlberg, M. Borgstrom, L. Montelius, W. Seifert, L. Samuelson, *Nano Lett.* **4**, 699 (2004). doi:[10.1021/nl035100s](https://doi.org/10.1021/nl035100s)
14. C.G. Jin, G.Q. Zhang, T. Qian, X.G. Li, Z. Yao, *J. Phys. Chem. B* **108**, 1844 (2004). doi:[10.1021/jp036133z](https://doi.org/10.1021/jp036133z)
15. T. Shimizu, T. Xie, J. Nishikawa, S. Shingubara, S. Senz, U. Gösele, *Adv. Mater.* **19**, 917 (2007). doi:[10.1002/adma.200700153](https://doi.org/10.1002/adma.200700153)
16. D. Zhao, J. Feng, Q. Huo, N. Melosh, G.H. Fredrickson, B.F. Chmelka, G.D. Stucky, *Science* **279**, 548 (1998). doi:[10.1126/science.279.5350.548](https://doi.org/10.1126/science.279.5350.548)
17. M.H. Huang, A. Choudrey, P. Yang, *Chem. Commun.* **12**, 1063 (2000). doi:[10.1039/b002549f](https://doi.org/10.1039/b002549f)
18. N.R.B. Coleman, N. O'Sullivan, K.M. Ryan, T.A. Crowley, M.A. Morris, T.R. Spalding, D.C. Steytler, J.D. Holmes, *J. Am. Chem. Soc.* **123**, 7010 (2001). doi:[10.1021/ja015833j](https://doi.org/10.1021/ja015833j)
19. R. Thiruvengadathan, O. Regev, *Chem. Mater.* **17**, 3281 (2005). doi:[10.1021/cm0500408](https://doi.org/10.1021/cm0500408)
20. S.Z. Wang, D.G. Choi, S.M. Yang, *Adv. Mater.* **14**, 1311 (2002). doi:[10.1002/1521-4095\(20020916\)14:18<1311::AID-ADMA1311>3.0.CO;2-R](https://doi.org/10.1002/1521-4095(20020916)14:18<1311::AID-ADMA1311>3.0.CO;2-R)
21. Y. Shi, Y. Wan, R. Liu, B. Tu, D. Zhao, *J. Am. Chem. Soc.* **129**, 9522 (2007). doi:[10.1021/ja072910n](https://doi.org/10.1021/ja072910n)
22. Z. konya, V.F. Puentes, I. Kiricsi, J. Zhu, A.P. Alivisatos, G.A. Somorjai, *Nano Lett.* **2**, 907 (2002). doi:[10.1021/nl0256661](https://doi.org/10.1021/nl0256661)
23. F. Gao, Q. Lu, D. Zhao, *Adv. Mater.* **15**, 739 (2003). doi:[10.1002/adma.200304758](https://doi.org/10.1002/adma.200304758)
24. S.M. Sze, *Physics of Semiconducting Devices*, 2nd edn. (Wiley, New York, 1981)
25. O. Harnack, C. Pacholski, H. Weller, A. Yasuda, J.M. Wessels, *Nano Lett.* **3**, 1097 (2003). doi:[10.1021/nl034240z](https://doi.org/10.1021/nl034240z)
26. L. Liao, K. Liu, W. Wang, X. Bai, E. Wang, Y. Liu, J. Li, C. Liu, *J. Am. Chem. Soc.* **129**, 9562 (2007). doi:[10.1021/ja072861e](https://doi.org/10.1021/ja072861e)
27. B.N. Pal, J. Sun, B.J. Jung, E. Choi, A.G. Andreou, H.E. Katz, *Adv. Mater.* **20**, 1023 (2008). doi:[10.1002/adma.200701550](https://doi.org/10.1002/adma.200701550)
28. K. Mohanta, A.J. Pal, *J. Phys. Chem. C* **112**, 3232 (2008). doi:[10.1021/jp076624+](https://doi.org/10.1021/jp076624+)
29. A. Datta, S.K. Panda, S. Chaudhuri, *J. Phys. Chem. C* **111**, 17260 (2007). doi:[10.1021/jp076093p](https://doi.org/10.1021/jp076093p)
30. Y.B. Guo, Q.X. Tang, H.B. Liu, Y.L. Li, W.P. Hu, S. Wang, D.B. Zhu, *J. Am. Chem. Soc.* **130**, 9198 (2008). doi:[10.1021/ja8021494](https://doi.org/10.1021/ja8021494)
31. Q.G. Li, R.M. Penner, *Nano Lett.* **5**, 1720 (2005). doi:[10.1021/nl050994x](https://doi.org/10.1021/nl050994x)
32. H. Li, J.M. Green, J. Jiao, *J. Phys. Chem. C* **112**, 15140 (2008). doi:[10.1021/jp804209j](https://doi.org/10.1021/jp804209j)
33. O. Hayden, R. Agarwal, C.M. Lieber, *Nat. Mater.* **5**, 352 (2006). doi:[10.1038/nmat1635](https://doi.org/10.1038/nmat1635)
34. N. Pradhan, B. Katz, S. Efrima, *J. Phys. Chem. B* **107**, 13843 (2003). doi:[10.1021/jp0357951](https://doi.org/10.1021/jp0357951)
35. P.A. Smith, C.D. Nordquist, T.N. Jackson, T.S. Mayer, *Appl. Phys. Lett.* **77**, 1399 (2000). doi:[10.1063/1.1290272](https://doi.org/10.1063/1.1290272)
36. L. Dong, J. Bush, V. Chirayos, R. Solanki, J. Jiao, Y. Ono, J.F. Conley Jr, B.D. Ulrich, *Nano Lett.* **5**, 2112 (2005). doi:[10.1021/nl051650+](https://doi.org/10.1021/nl051650+)
37. X.Q. Chen, T. Saito, H. Yamada, K. Matsushige, *Appl. Phys. Lett.* **78**, 3714 (2001). doi:[10.1063/1.1377627](https://doi.org/10.1063/1.1377627)
38. Z. Chen, Y. Yang, F. Chen, Q. Qing, Z. Wu, Z. Liu, *J. Phys. Chem. B* **109**, 11420 (2005). doi:[10.1021/jp051848i](https://doi.org/10.1021/jp051848i)
39. A. Vijayaraghavan, S. Blatt, D. Weissenberger, M. Oron-Carl, F. Hennrich, D. Gerthsen, H. Hahn, R. Krupke, *Nano Lett.* **7**, 1556 (2007). doi:[10.1021/nl0703727](https://doi.org/10.1021/nl0703727)
40. C.S. Lao, J. Liu, P. Gao, L. Zhang, D. Davidovic, R. Tummala, Z.L. Wang, *Nano Lett.* **6**, 263 (2006). doi:[10.1021/nl052239p](https://doi.org/10.1021/nl052239p)
41. G. Cheng, S.J. Wang, K. Cheng, X.H. Jiang, L.X. Wang, L.S. Li, Z.L. Du, G.T. Zou, *Appl. Phys. Lett.* **92**, 223116 (2008). doi:[10.1063/1.2938694](https://doi.org/10.1063/1.2938694)
42. G. Cheng, Z.H. Li, S.J. Wang, H.C. Gong, K. Cheng, X.H. Jiang, S.M. Zhou, Z.L. Du, T. Cui, G.T. Zou, *Appl. Phys. Lett.* **93**, 123103 (2008). doi:[10.1063/1.2989129](https://doi.org/10.1063/1.2989129)
43. C.Y. Nam, D. Tham, J.E. Fischer, *Nano Lett.* **5**, 2029 (2005). doi:[10.1021/nl0515697](https://doi.org/10.1021/nl0515697)
44. Z.Y. Zhang, C.H. Jin, X.L. Liang, Q. Chen, L.M. Penga, *Appl. Phys. Lett.* **88**, 073102 (2006). doi:[10.1063/1.2177362](https://doi.org/10.1063/1.2177362)
45. H. Bao, X. Cui, C. Li, Y. Gan, J. Zhang, J. Guo, *J. Phys. Chem. C* **111**, 12 (2007)